Chitin utilization by marine picocyanobacteria and the evolution of a planktonic lifestyle

Giovanna Capovilla†*[1], Rogier Braakman†*[2], Gregory Fournier[2], Thomas Hackl[1,3], Julia Schwartzman[1], Xinda Lu[1,4], Alexis Yelton[1,5], Krista Longnecker[6], Melissa Kido Soule[6], Elaina Thomas[1,7], Gretchen Swarr[6], Alessandro Mongera[8,9], Jack Payette[2], Jacob Waldbauer[10], Elizabeth B. Kujawinski[6], Otto X. Cordero[1], Sallie W. Chisholm*[1,11]

[1]Department of Civil & Environmental Engineering, Massachusetts Institute of Technology, Cambridge, MA, USA

[2] Department of Earth, Atmospheric and Planetary Sciences, Massachusetts Institute of Technology, Cambridge, MA, USA

[3] Groningen Institute of Evolutionary Life Sciences, University of Groningen, Groningen, Netherlands

[4] present address: DermBiont Inc., Boston, MA, United States

[5] present address: ActZero.ai, Seattle, WA, United States

[6] Department of Marine Chemistry and Geochemistry, Woods Hole Oceanographic Institution, Woods Hole, MA, USA

[7] present address: School of Oceanography, University of Washington, Seattle, WA, USA

[8] Department of Pathology, Brigham and Women's Hospital, Boston, MA, USA

[9] Department of Genetics, Harvard Medical School, Boston, MA, USA

[10] Department of the Geophysical Sciences, University of Chicago, Chicago, IL, USA

[11] Department of Biology, Massachusetts Institute of Technology, Cambridge, MA, USA

† Equal contributions

* Corresponding authors
Giovanna Capovilla (giocapo@mit.edu)
Rogier Braakman (braakman@mit.edu)
Sallie W. Chisholm (chisholm@mit.edu)

ABSTRACT

Marine picocyanobacteria (*Prochlorococcus* and *Synechococcus*), the most abundant photosynthetic cells in the oceans, are generally thought to have a primarily single-celled and free-living lifestyle. However, we find that genes for breaking down chitin - an abundant source of organic carbon that primarily exists as particles - are widespread in this group. We further show that cells with a chitin degradation pathway display chitin degradation activity, attach to chitin particles and show enhanced growth under low light conditions when exposed to chitosan, a partially deacetylated form of chitin. Marine chitin is largely derived from arthropods, whose roots lie in the early

Phanerozoic, 520-535 million years ago, close to when marine picocyanobacteria began colonizing the ocean. We postulate that attachment to chitin particles allowed benthic cyanobacteria to emulate their mat-based lifestyle in the water column, initiating their expansion into the open ocean, seeding the rise of modern marine ecosystems. Transitioning to a constitutive planktonic life without chitin associations along a major early branch within the *Prochlorococcus* tree led to cellular and genomic streamlining. Our work highlights how coevolution across trophic levels creates metabolic opportunities and drives biospheric expansions.

Prochlorococcus and its sister lineage marine *Synechococcus* (together 'marine picocyanobacteria') are a monophyletic and highly abundant group of oceanic phytoplankton that perform about ~25% of oceanic CO_2-fixation(1–3). In addition to their role as primary producers, it is increasingly clear that marine picocyanobacteria also use organic carbon as a supplemental carbon and energy source (i.e. mixotrophy)(4–6), especially in the light-limited deep euphotic zone(7, 8). While studying genes involved in mixotrophy in this group(9), we noticed that some strains have chitinase genes, indicating the potential for using chitin, one of the most abundant sources of organic carbon in the ocean(10, 11). However, chitin in the marine environment typically exists as particles, primarily derived from arthropod exoskeletons(10, 11), which are broken down by microbial consortia(12). Marine picocyanobacteria are typically considered to live an exclusively single-celled planktonic lifestyle(13, 14), but are also sometimes found within particulate organic matter aggregates(15) that sink out of the euphotic zone(16). Together this suggests that chitin utilization might be a functional trait in marine picocyanobacteria.

To explore this possibility we began by examining the distribution of genes involved in chitin utilization in *Prochlorococcus* and *Synechococcus* genomes (Fig. 1). This comparison is complicated by the significant overlap in gene content between pathways for chitin utilization and peptidoglycan recycling (Fig. 1). Peptidoglycan, which is chemically similar to chitin, forms a single cell-size polymeric structure (the sacculus) that is a component of the bacterial cell wall, and recycling of peptidoglycan fragments inevitably generated during cell growth and division is widespread in bacteria(17). We therefore searched 702 partial and complete genomes for genes required for both chitin utilization and peptidoglycan recycling. We found that in *Synechococcus* and deeply branching "low-light-adapted IV" (LLIV) *Prochlorococcus* most of these genes are nearly universal, i.e. they occur at a frequency similar to the average genome completeness of ~75% (Methods) (Fig. 1). In contrast, these genes are almost universally absent in "high-light-adapted" (HL) *Prochlorococcus* (Fig. 1). All LL clades of *Prochlorococcus* possess peptidoglycan recycling genes, but chitin utilization genes are nearly exclusive to the deeply branching LLIV clade (Fig. 1). These observations suggest that chitin utilization and peptidoglycan recycling were both present in the last common ancestor of marine picocyanobacteria, but were lost during the diversification of extant *Prochlorococcus* groups.

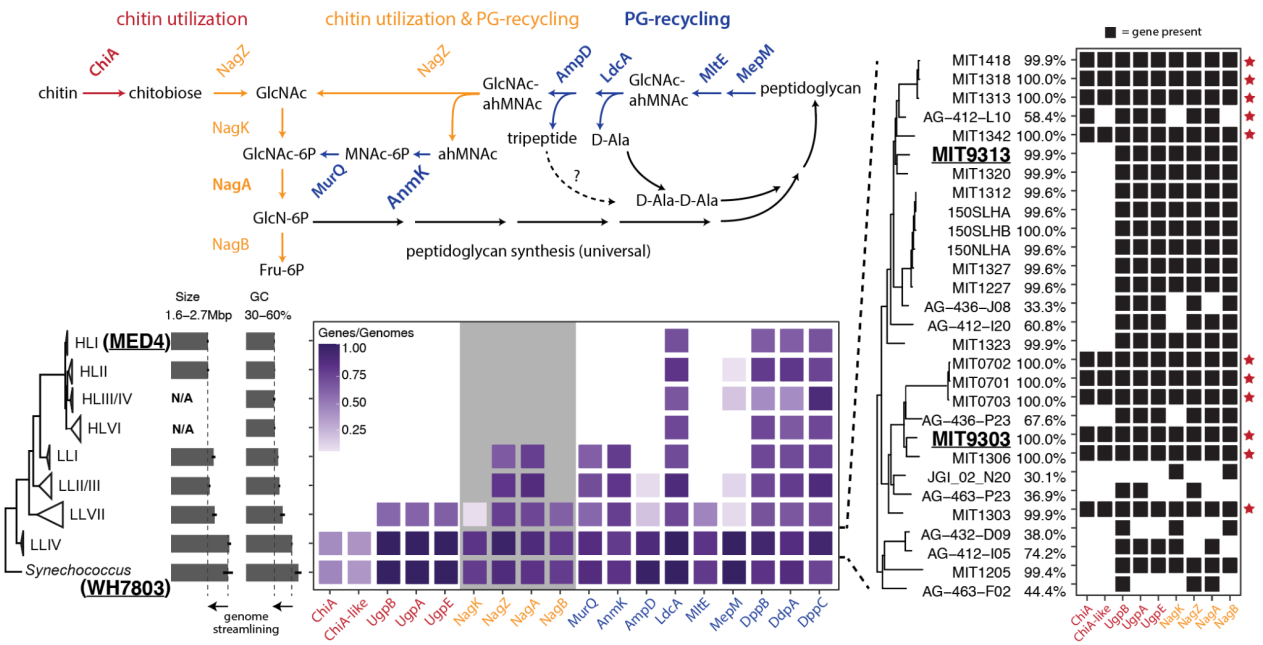

Figure 1. Distribution of chitin utilization genes in marine picocyanobacteria. Upper panel: Pathway for chitin degradation (red) and its reactions that overlap (orange) with peptidoglycan metabolic recycling (blue). ChiA is annotated as a putative chitinase enzyme, while ChiA-like is a homolog of the substrate-binding domain of ChiA and annotated as a putative chitin-binding domain protein. Lower panel: Average frequency of occurrence of chitin utilization and peptidoglycan recycling genes estimated from both partial and complete genome sequences available in *Synechococcus* and the major clades of *Prochlorococcus* shown in the tree on the left. Average completeness of genomes in our sample is ~75% (see Methods). The clade-membership of the strains used in the experiments are highlighted in bold and underlined. The grey background area in the gene frequency frame highlights genes shared between the chitin utilization and peptidoglycan pathways (orange). The panel on the right breaks down members of the LLIV clade of *Prochlorococcus,* revealing putative primary chitin degraders of chitin that possess chitinase (red star) and putative secondary degraders that lack chitinase. Abbreviations: GlcNAc - N-acetyl-glucosamine, GlcNAc-6P - N-acetyl-glucosamine 6-phosphate, GlcN-6P - glucosamine 6-phosphate, F6P - fructose 6-phosphate, ahMNAc - anhydro-N-acetyl-beta-muramate, MNAc-6P - N-acetyl-muramate 6 phosphate.

In both *Prochlorococcus* and *Synechococcus*, genomes containing chitin-utilization genes sub-differentiate into two groups, which either possess or lack chitinase, the enzyme that hydrolyzes chitin(Fig. 1). It is known from other systems that chitin utilization is a complex ecological process(18, 19) with hydrolysis of chitin polymers occurring in the extracellular milieu, making chitin fragments available to all cells in the community. Consequently, chitin breakdown involves niche partitioning into groups that specialize in performing the initial hydrolysis steps and others that specialize in using small chitin oligosaccharides(20). Our results suggest a similar niche partitioning into ‘primary’ and ‘secondary’ degraders may occur among chitin-using members of the marine picocyanobacteria.

To determine whether the putative chitin users (Fig. 1) actually metabolize chitin, we first used enzyme assays to examine whether the cells display chitinase activity. Both *Synechococcus* and *Prochlorococcus* strains that are putative primary degraders of chitin (i.e. possessing the full complement of chitin utilization genes) displayed chitinase activity in cell-free spent media, and the activity disappeared upon boiling the media (Fig. 2, S1) – consistent with the production of extracellular chitinase enzymes that are denatured upon heating. In agreement with the genomic predictions, a *Prochlorococcus* strain (MIT9313, Fig. 1) that is a

122 putative secondary chitin degrader did not display extracellular chitinase activity in spent
123 media (Fig. 2, S1).
124
125

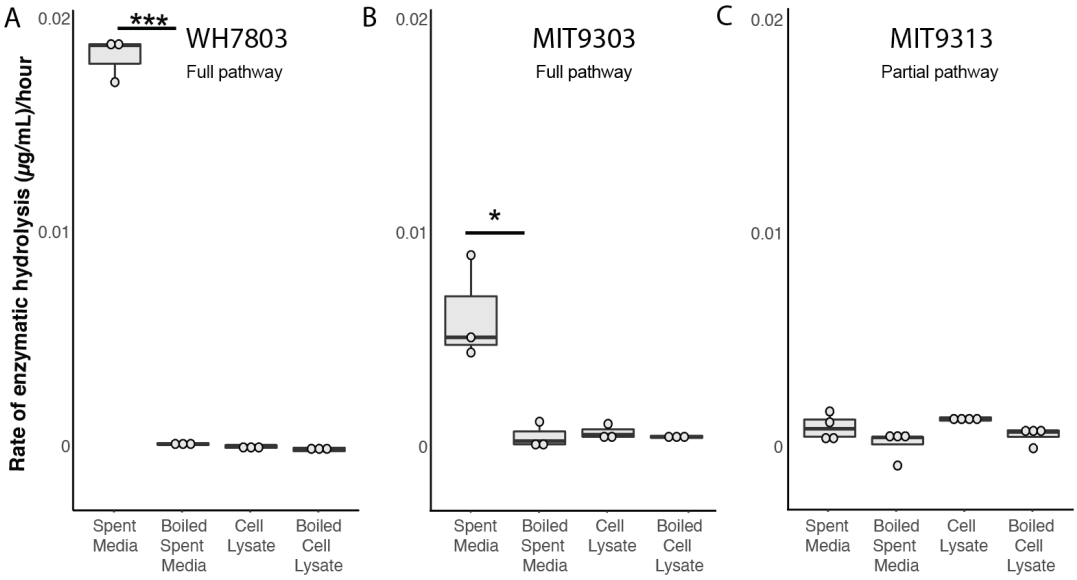

126
127 **Figure 2. Chitinase activity in *Prochlorococcus* and *Synechococcus*.** Endochitinase activity in
128 *Synechococcus* WH7803, *Prochlorococcus* MIT9303, and *Prochlorococcus* MIT9313 measured in spent media
129 and cell lysates. Strains with the complete chitin degradation pathway display such activity in the spent media.
130 Activity is lost after boiling. Exochitinase activity is shown in Figure S1.
131
132 The next question we addressed was whether or not *Synechococcus* and *Prochlorococcus*
133 cells with the chitin utilization pathway colonize chitin surfaces, by adding hydrogel chitin
134 beads to cultures. The *Prochlorococcus* strains used were from the two sub-groups we
135 identified as putative primary (MIT9303) and secondary (MIT9313) degraders (Fig. 1), as
136 well as cells lacking the complete pathway for chitin degradation (MED4). The
137 *Synechococcus* strain used was WH7803, a primary chitin degrader with a complete set of
138 chitin utilization genes. We found that both *Synechococcus* and *Prochlorococcus* cells with
139 chitin utilization genes attach to chitin particles, while *Prochlorococcus* lacking chitin
140 degradation genes do not (Fig. 3). Primary degraders attach both to the surface of particles
141 and accumulate in "pockets" within the beads (Fig. 3A,C,D,F), while secondary degraders
142 only accumulate in pockets (Fig. 3A,B,F), potentially reflecting the inferred niche
143 partitioning between them. Finally, we found that *Prochlorococcus* attaches only to chitin
144 particles and not to agarose, but that *Synechococcus* attaches to both (Fig. 3A, S2), suggesting
145 that *Synechococcus* has broader surface attachment abilities than *Prochlorococcus.*

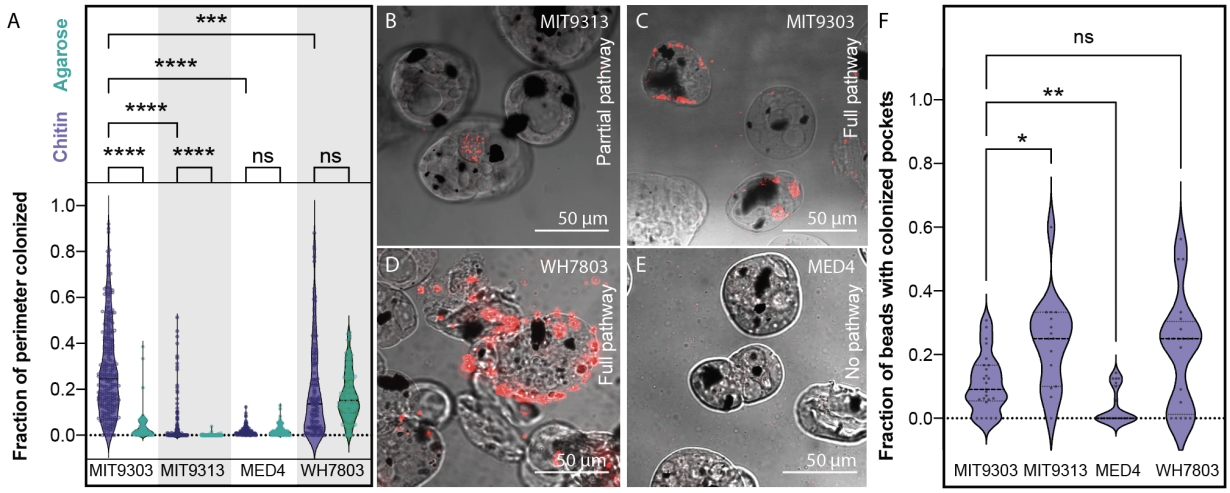

Figure 3. Colonization of artificial chitin particles by *Prochlorococcus* and *Synechococcus*. A) Fraction of particle perimeter colonized by a strain of *Synechococcus* (WH7803) and 3 strains of *Prochlorococcus* (MED4, MIT 9313, and MIT 9303) exposed to agarose (green) and chitin (purple) particles. *Synechococcus* WH7803 and *Prochlorococcus* MIT9303 are putative primary chitin degraders, *Prochlorococcus* MIT9313 is a putative secondary chitin degrader (i.e. it lacks chitinase), and *Prochlorococcus* MED4 lacks all chitin degradation genes. B-E). Confocal sections of chitin particles quantified in A. Chitin particles are shown in bright field mode; the dark spots are magnetic beads embedded in the particles. *Synechococcus* and *Prochlorococcus* are detected by their red autofluorescence. Cells were sometimes observed contained in pockets within the particles (as shown in B and C, for example). Quantification of this phenomenon is shown in F.

As a material resource, chitin potentially provides energy, carbon, and/or nitrogen. *Prochlorococcus* niche partitioning provides relevant clues on what it derives from chitin, as chitin utilization is only retained within the LLIV clade (Fig. 1), which dominates at the bottom of the euphotic zone(21). At these depths, light goes to extinction and *Prochlorococcus* is thought to derive a significant fraction of its carbon through mixotrophy rather than photosynthesis(7, 8). This suggests chitin could provide *Prochlorococcus* a supplemental carbon and energy source that is beneficial under low light conditions. To test this hypothesis, we grew *Prochlorococcus* cells representing both the primary and secondary degrader genotypes (Fig. 1) at several light levels, with and without the addition of chitosan, a form of chitin that is solubilized through partial deacetylation. Differences due to chitosan additions emerged only at the lowest light level (Fig. 4), and for primary degraders was expressed as a higher growth rate, albeit not significantly so, while for secondary degraders was expressed as a higher cell density in stationary phase, potentially reflecting their niche partitioning. A growth boost due to chitin utilization only under light-limitation is consistent with results in other cyanobacteria showing that wild-type cells able to recycle peptidoglycan fragments generated during the normal course of growth have higher growth rates than mutants without this ability, but only at low light levels(22). We also examined whether *Prochlorococcus* can use chitosan as a source of nitrogen by adding it to the growth media of nitrogen-starved cells, but relief from nitrogen stress was not apparent (Fig. S3, S4). Together, this suggests that in its role as a resource, chitin primarily acts as a supplemental carbon source to light-limited *Prochlorococcus* cells deep in the water column.

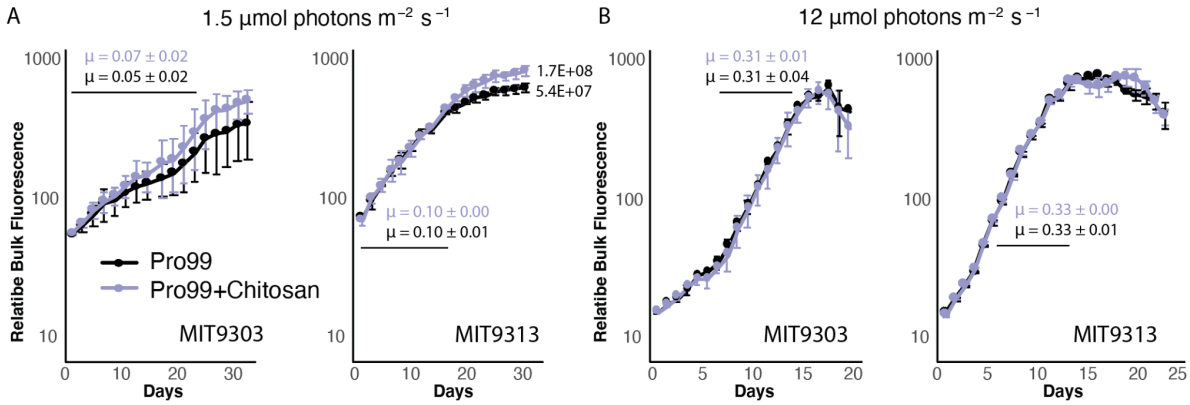

Figure 4. Effect of chitosan addition on growth of two *Prochlorococcus* strains as a function of light intensity. MIT9303 is a primary chitinase degrader and MIT9313 is a secondary degrader, missing the chitinase genes. Cultures were grown in Pro99 media with (purple) and without (black) added chitosan, at two different light intensities: 1.5 µmol photons m^{-1} s^{-1} (A) and 12 µmol photons m^{-1} s^{-1} (B), the former being growth-limiting for these strains as reflected in the difference in growth rates, µ, at the different light levels. Growth was monitored by bulk chlorophyll fluorescence, but upon emergence of a significant difference in fluorescence in MIT9313 cultures cell counts were measured using flow cytometry. Chitosan-amended cultures had higher cell counts in stationary phase (1.7E+8 cells mL^{-1}) than unamended cultures (5.4E+7 cells mL^{-1}), reflecting an increase in cell yield. Error bars show standard deviation between the 3 biological replicates. The average growth rate and associated standard deviation (µ, in units day^{-1}) was calculated in exponential phase (marked with a black line) and is shown for each curve.

To investigate how cells respond to chitin addition at the molecular level, we used qPCR to measure the expression of genes in the chitin degradation pathway in *Prochlorococcus* cultures grown with and without chitosan. All genes were expressed under both conditions (Table S3), including the chitinase and chitobiose transporter genes that are specific to chitin degradation (Fig. 5A). This suggests cells constitutively express this pathway, perhaps so they are poised to use chitin when it appears in the environment. Furthermore, while changes in expression due to chitosan exposure were not statistically significant for most genes, we observed a clear trend across the full suite of genes. That is, shortly after chitosan addition, expression of chitinase genes was higher relative to unamended cultures, while expression of downstream genes was lower (Fig. 5A). At later time points, the expression of chitinase was lower and downstream genes higher in amended relative to unamended cultures (Fig. 5A). These patterns suggest that *Prochlorococcus* cells increase the activity of chitin degradation enzymes in the order in which pathway intermediates become available, which is broadly similar to how chitin degradation pathways operate in other chitinolytic bacteria(23).

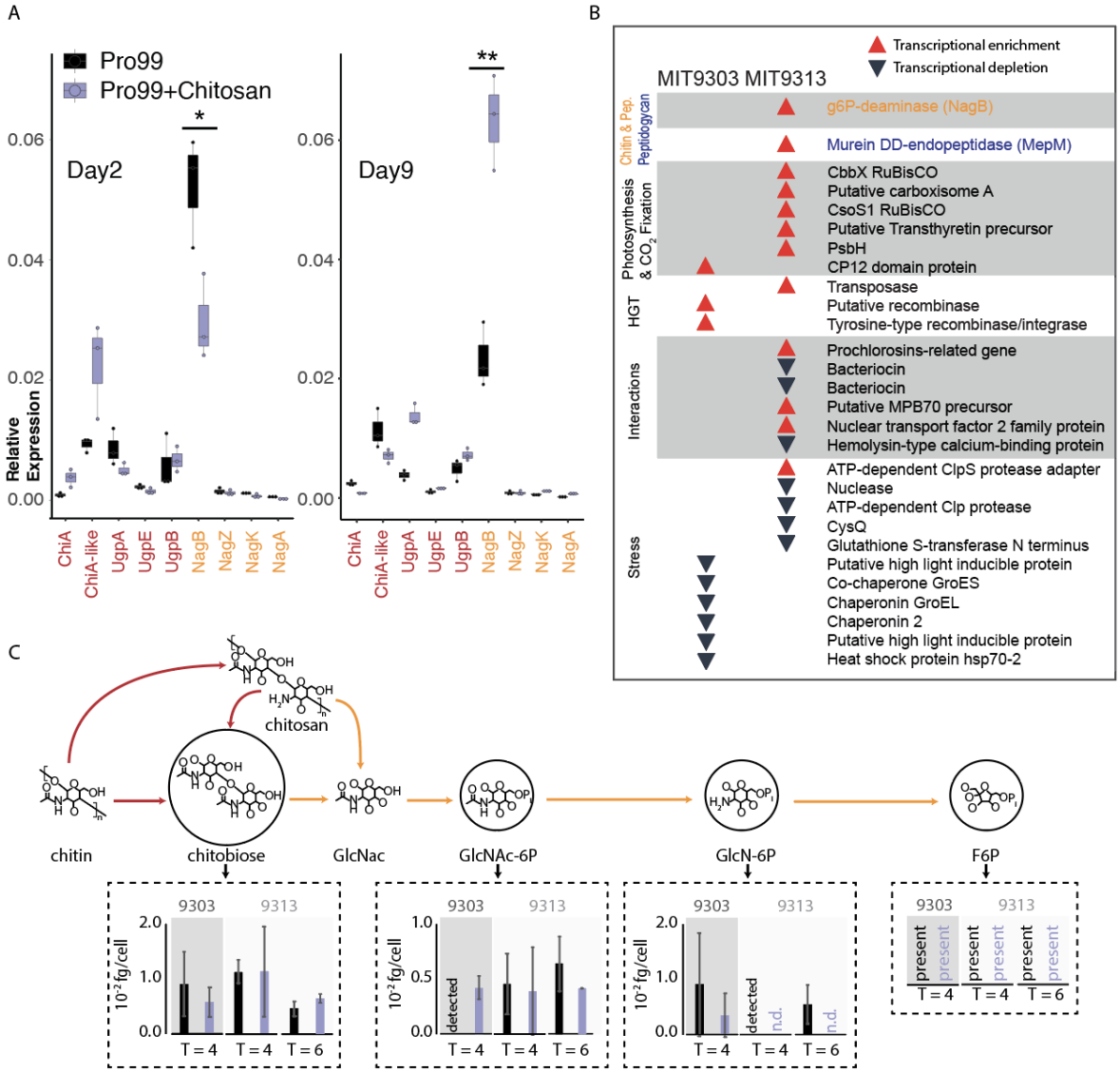

Figure 5. Gene expression and metabolomic analysis in *Prochlorococcus* in response to the addition of chitosan. A) Expression (measured by qPCR) of all the chitin-related genes in MIT9303 (primary degrader) in relation to the housekeeping gene, *rnpB,* gene in natural seawater-based Pro99 medium in presence and absence of chitosan at two time points over the growth curve. Cells were in early exponential growth on Day 2 and mid-exponential on Day 9. B) Qualitative representation of the relative expression of genes (measured using RNA-Seq) in the two *Prochlorococcus* strains 24 hours after addition to chitosan (see also Fig. S5). Red upward pointing arrows represent statistically significant transcript enrichment in presence of chitosan while black downward pointing arrows represent statistically significant transcript depletion. Genes are grouped by functional categories, which are shown in shaded/unshaded sections. C) Concentrations of intermediates of chitin degradation on days 4 and 6 after chitosan additions (purple) compared to unamended controls (black). Error bars show the standard deviations of 3 biological replicates for MIT9303 and MIT9313 on day 4, and of 2 replicates for MIT9313 on day 6. Molecular abbreviations and color scheme is the same as in Fig. 1. Metabolites are labeled as 'detected' in samples where they were observed in only a single replicate, and as 'n.d.' (not detected) in samples where they were not observed in any replicates. Fructose-6-P was present in most samples, but its levels could not be quantified due to interference by the organic carbon matrix.

To augment the qPCR results and gain a systems-level understanding of how the availability of chitin shapes *Prochlorococcus,* we performed RNA-Seq and metabolomic analyses of

233 cultures exposed to chitosan. While expression of many genes changed in response to the
234 addition of chitosan, relatively few of those changes were significant, and they disappeared
235 after 48 hours (Fig. 5B, S5). As with our analysis of the expression of individual genes by
236 qPCR, this suggests a mild and transient response to chitosan additions. We further observed
237 transcripts of all genes of the chitin utilization pathway and accumulation of all its metabolic
238 intermediates under all conditions (Fig. 5C, Table S3,S4), consistent with the idea that cells
239 constitutively express this pathway to be ready when chitin appears in the environment, as
240 also suggested by qPCR data (Fig. 5A).
241
242 While the chitin utilization pathway is always active, *Prochlorococcus* metabolism also
243 responds to chitosan additions: in one strain, MIT9313 (secondary degrader), the expression
244 of two genes involved in peptidoglycan recycling (NagB, MepM), one of which is also
245 involved in chitin utilization (NagB), significantly increased (Fig. 5B), consistent with the
246 noted molecular, physiological and ecological links between pathways (Fig. 1). Similarly,
247 concentrations of chitin degradation intermediates also changed upon addition of chitosan,
248 although most changes were not significant (Fig. 3C). Additional changes occurred in
249 downstream metabolic processes. Transcripts of several genes involved in photosynthesis and
250 carbon fixation were enriched in the presence of chitosan in MIT9313, a secondary degrader
251 of chitin, which could have indirectly contributed to the difference in cell number observed in
252 low light levels (Fig. 4A). Transcripts for CP12, which inhibits carbon fixation(24), were
253 enriched in the presence of chitosan in MIT9303, a primary degrader of chitin (Fig. 1,3B).
254 Furthermore, the concentration of several intermediates of core carbohydrate metabolism
255 changed in the presence of chitosan (Fig S6), although again few changes were significant.
256 Together these observations indicate that chitosan exposure modifies the processing of
257 carbon through core metabolic pathways.
258
259 Changes in a number of other functional categories in cells exposed to chitosan can be
260 grouped together in terms of their inferred ecological function. Transcripts of various genes
261 involved in horizontal gene transfer (e.g., transposases and recombinases), and microbial
262 interactions (e.g., antibiotics, lanthipeptides, secreted proteins) were enriched, while
263 transcripts of various genes involved in mitigating stress (e.g., chaperonins, high light-
264 inducible proteins, proteases, and genes related to glutathione) were depleted (Fig. 3B, S5).
265 Since life in biofilms increases microbial interactions, promotes horizontal gene transfer(25),
266 helps buffer against external stresses(26), and increases likelihood of the light-limited
267 conditions under which peptidoglycan recycling becomes beneficial(22), we interpret these
268 collective changes as cells preparing to attach to chitin particles and switch to a surface-
269 attached lifestyle.
270
271 To gain insight into the Earth-historical context of the acquisition of the chitin utilization trait
272 in *Prochlorococcus* and *Synechococcus*, we examined when this acquisition happened
273 relative to the divergence of marine picocyanobacteria from other cyanobacteria.
274 Picocyanobacterial sequences for most genes involved in both the chitin degradation and
275 peptidoglycan recycling pathways (i.e. orange genes in Fig. 1) are nested within larger
276 branches of cyanobacterial genes (Fig. 6, S7), indicating ancestral vertical inheritance of
277 peptidoglycan recycling. In contrast, picocyanobacterial sequences for both chitinase (ChiA
278 and ChiA-like) and N-acetylglucosamine kinase (NagK) are nested within non-cyanobacterial
279 diversity, indicating horizontal gene transfer to picocyanobacteria after their divergence from
280 other cyanobacteria (Fig. 6, S7). NagK is present in deeply branching 'SynPro' groups (i.e.,
281 including *Cyanobium* and related *Synechococcus* that bridge the fresh-salt water divide), but
282 chitinase genes are exclusive to 'marine SynPro' (Fig. 6, S7). NagK fortifies peptidoglycan

283 recycling by completing a second branch involved in metabolizing GlcNAc but is obligately
284 required for chitin utilization (Fig. 1,7A). These observations suggest that peptidoglycan
285 recycling pre-dated the radiation of marine picocyanobacteria and provided a preadaptation to
286 chitin utilization. Acquisition of chitinase along the stem leading from total group SynPro to
287 crown-group marine SynPro then enabled chitin utilization by this group (Fig. 7A).

NagK

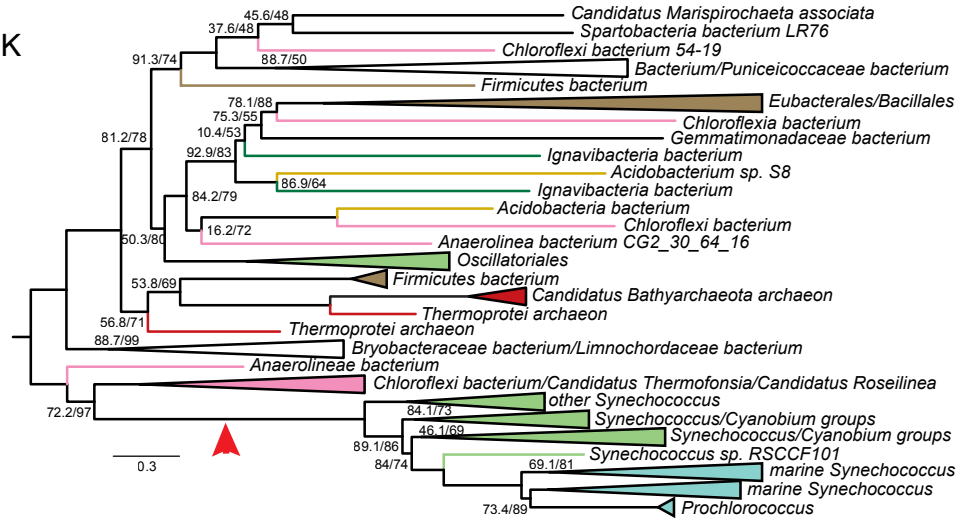

ChiA domain

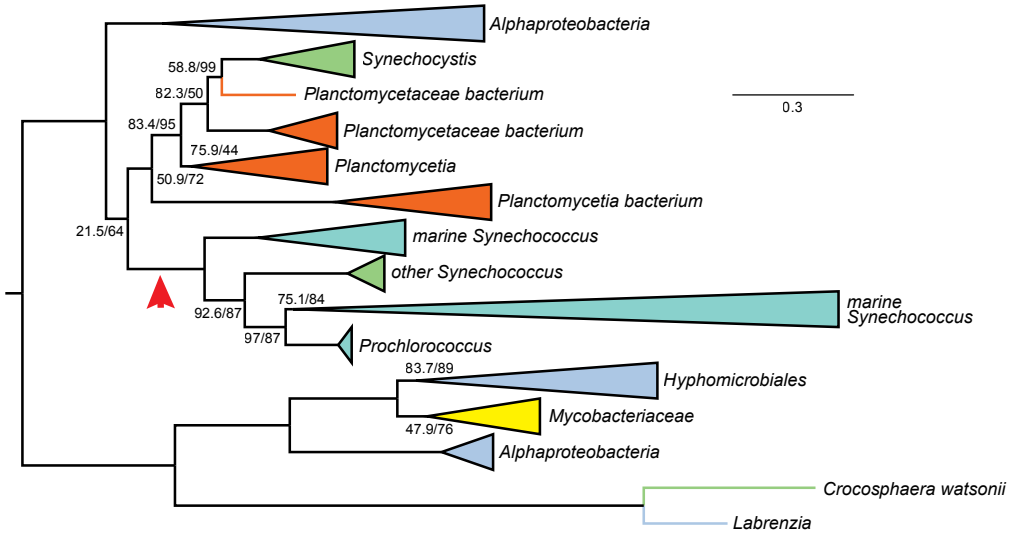

ChiA domain

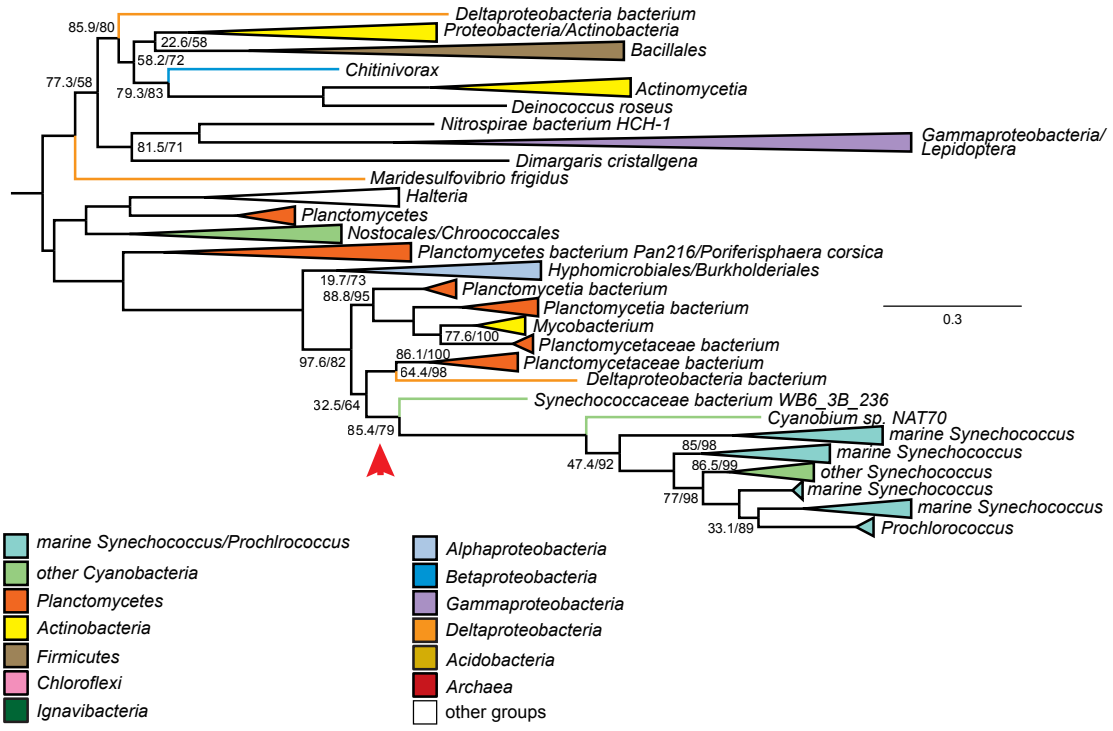

289
290 **Figure 6. Phylogenies of ChiA and NagK genes in marine picocyanobacteria.** Red arrows
291 indicate inferred HGTs into SynPro ancestor lineages. Branch lengths are indicated by included scale bars
292 (average substitutions/site). High-level taxonomic identities are indicated by color coding, with specific
293 represented groups labeled for terminal and collapsed groups. In each case, trees are rooted at the branch closest
294 to the midpoint that preserves the monophyly of Synechococcales groups including SynPro. Branch supports
295 (approximate likelihood ratio test/bootstrap value) are included for bipartitions with less than 90% support for
296 either metric. Phylogenies of NagZ, NagA, NagB, UgpA, and UgpB are found in Figure S7.
297
298
299

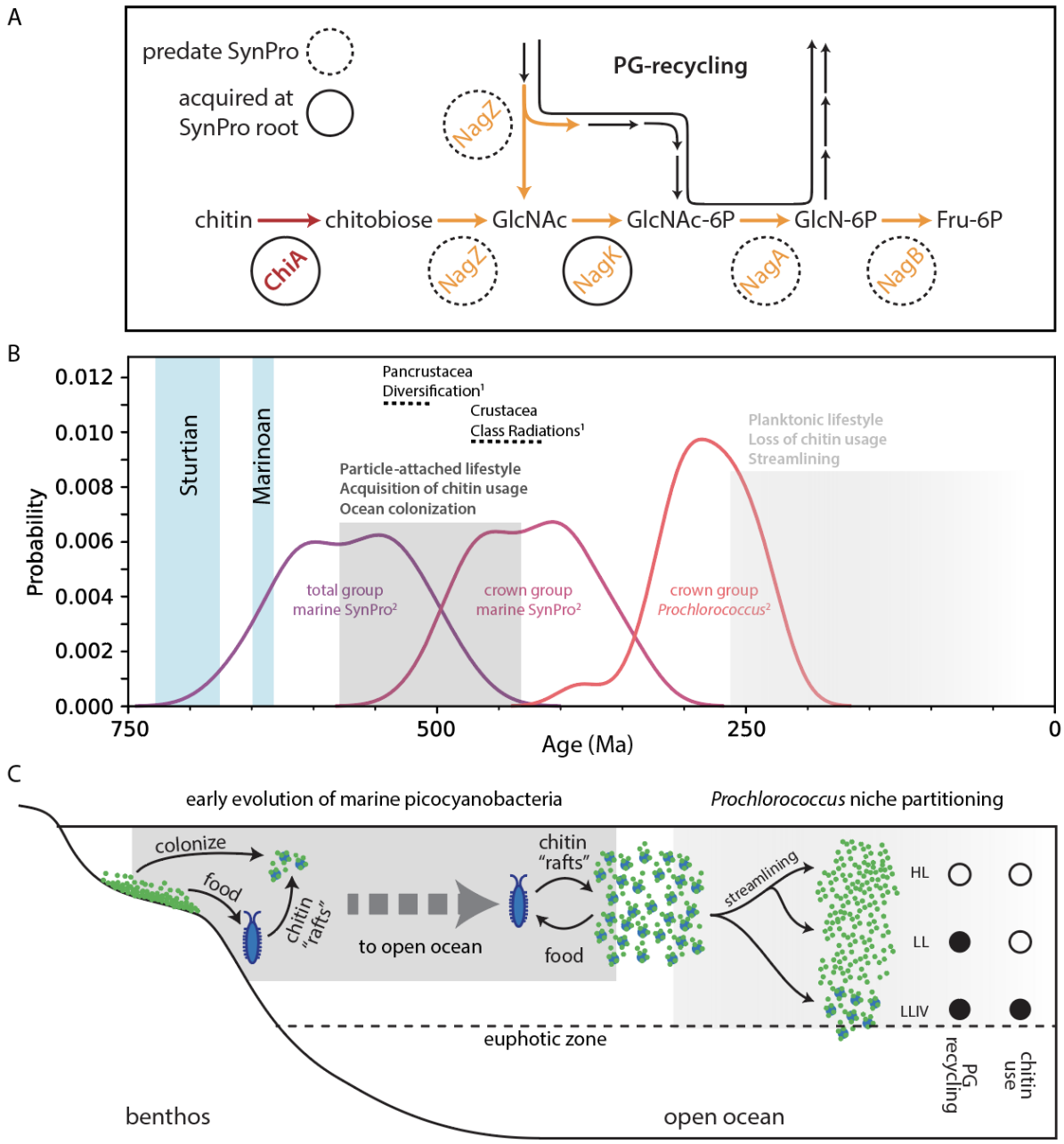

300
301
302 **Figure 7. Hypothesized timing and ecological context of the rise of marine**
303 **picocyanobacteria.** A) Pathways for chitin utilization and peptidoglycan metabolic recycling. Genes
304 exclusive to chitin utilization are shown in red, and genes shared between the two pathways are shown in
305 orange. Genes highlighted with dashed circles pre-date evolution of marine picocyanobacteria, while genes
306 highlighted with solid circles were acquired along the stem leading to their crown group. B) Summary of

divergence time estimates for the evolution of 1) arthropods(27) and 2) marine picocyanobacteria(28), which we postulate are linked via chitin utilization metabolism. Vertical blue bars represent the snowball Earth intervals preceding the rise of marine picocyanobacteria. C) The "chitin-raft hypothesis" for the rise of marine picocyanobacteria. The rise of marine arthropods led to an accumulation of chitin in the environment, providing a substrate that benthic cyanobacteria could colonize while preserving their surface-attached lifestyle. Existing peptidoglycan recycling pathways provided a preadaptation for acquiring chitin degradation pathways (Fig. 7A). As *Prochlorococcus* diversified, loss of chitin associations and adaptation to a constitutive planktonic lifestyle occurred during cellular and genomic streamlining, and a shift from physical-chemical interactions within particle-attached communities to purely chemical interactions in the water column. A facultative ability to colonize chitin particles and use chitin as a supplemental carbon source under light limitation was preserved in the LLIV clade of *Prochlorococcus* that is adapted to the low light conditions at the bottom of the euphotic zone.

To better understand the context of the transfer of chitinase genes into ancestors of marine SynPro we examined their phylogenetic relationships to similar sequences found within other bacterial groups. Picocyanobacterial chitinases contain two major chitin-binding domains that show homology to different chitinase sequence variants found within other bacterial genomes. Gene sequence alignments suggest that the marine SynPro variant is likely the product of a fusion of two genes that were both acquired from Planctomycetes (SI Text 1). However, the sampling of Planctomycete diversity is too sparse to determine if the gene fusion event occurred before or after the transfers into ancestral marine SynPro (see SI Text 1 and SI Text 1 files for detailed discussion). Planctomycete genomes and metagenomes containing chitinases are found in both fresh and marine environments, preventing us from determining if the gene transfers to picocyanobacteria occurred in freshwater environments prior to colonization of the ocean, or within the marine planktonic environment. Recipients of chitinase genes from Planctomycetes include both marine and freshwater bacteria (SI Text 1), suggesting the lack of a strong congruence between ecological and phylogenetic signals.

Palaeobiological evidence provides further insight into the early evolution of chitin utilization in marine picocyanobacteria. First, molecular clocks constrained by horizontally transferred genes that link the timing of cyanobacterial evolution to that of other bacterial phyla indicate that the stem lineage leading to crown group SynPro existed during the interval of ~570-420 Ma(28) (Fig. 7B). Second, both fossils and fossil-calibrated molecular clocks indicate that marine arthropods – whose exoskeletons are the main source of chitin in the ocean(10, 11) – underwent a major ecological expansion between ~535-400 Ma(27, 29, 30). Finally, while the body fossil record from open ocean environments is limited because of a high likelihood of degradation before preservation, the second half of this period (~480-400 Ma), nearer to the calculated timing of crown group SynPro (Fig. 7B), is thought to have seen an increase in pelagic planktonic arthropods(31) and the emergence of more complex trophic structures in the open ocean(31–34). These dates are consistent with the hypothesis that the early evolution of marine picocyanobacteria and arthropods was intertwined, and played a role in establishing modern marine ecosystems.

Given chitin utilization by marine picocyanobacteria and their apparent contemporaneous evolution with arthropods, one might expect existence of direct associations with arthropods in the extant biosphere. However, while *Synechococcus* has been found to be abundant in copepod guts (35), we found no reports of direct associations with the exoskeletons of living copepods or other arthropods(35, 36). It is possible that chitin utilization by picocyanobacteria has become primarily restricted to detrital particulate matter, derived from exoskeletal molts (which constitute the largest flux of arthropod chitin into the environment) and dead bodies. Alternatively, direct arthropod-picocyanobacterial associations may yet be

discovered now that there is added motivation to look for them. Indeed, picocyanobacterial symbionts have been discovered in association with an increasingly diverse set of algae in recent years, including dinoflagellates, foraminifera, radiolarians, and tintinnids(15, 37–41).

The emergence of chitin attachment and utilization during the rise of marine picocyanobacteria helps address a conundrum regarding the evolution of lifestyle in this group. In most environments other than lakes and oceans, microbes predominantly live as aggregates attached to surfaces, which provides protection from external stresses and allows efficient recycling of nutrients(26). The earliest marine cyanobacteria likely also predominantly lived in mats in the benthic environment(13, 42–44). In contrast, extant marine picocyanobacteria are generally thought to live a single-celled planktonic life(13, 14), despite existing in a saline, UV-rich, and nutrient-poor environment, which are all factors associated with inducing aggregation of cells and attachment to surfaces(26, 45–47). This raises the question: what was the sequence of innovations that allowed cyanobacteria to make the evolutionary transition from life in benthic mats to life as individual planktonic cells in the open ocean?

To resolve this conundrum, we propose the "chitin raft hypothesis", in which picocyanobacteria and arthropods colonized the open ocean in tandem (Fig. 7C). Accumulated detrital chitin and other organic material could have provided "rafts" that allowed picocyanobacteria to maintain a surface-attached lifestyle while expanding into the ocean. By promoting collective nutrient recycling and stress mitigation, life in chitin particle-attached communities would have provided refugia from the harsh environment of the open ocean, allowing cells over millions of years of evolution to acquire necessary adaptations for an eventual transition to a single-celled planktonic life. Indeed, evolution of marine picocyanobacteria involved acquisition of genes for synthesis of unique compatible solutes for mitigating osmotic stress in saline environments(48, 49), various genes involved in mitigating light/UV stress or repairing light damage(50, 51), a number of changes to the membrane, genome, and proteome that are thought to lower cellular nutrient requirements(52–54), and a general remodeling of metabolism that is thought to enhance cellular nutrient affinity(55). Each of these innovations acts to mitigate against stresses that in other contexts are linked to triggering aggregation of cells and attachment to surfaces(26, 45–47).

This sequence of innovations culminated with a period of dramatic genomic and proteomic streamlining(52, 54) (Fig. 1) and enhanced genetic drift(56) along the branch separating the LLIV clade and all other *Prochlorococcus*, indicating the occurrence of a major population bottleneck. This transition also involved a shift in other *Prochlorococcus* lineages toward a smaller and rounder cell(57, 58) and the loss of both chitin utilization genes (Fig. 1) and the ability to attach to chitin particles (eg. MED4 in Fig. 3). Together these observations lead us to conclude that the divergence between LLIV and other *Prochlorococcus* involved a transition from a facultatively particle-attached to a constitutively planktonic lifestyle. Metabolic reconstructions indicate that streamlining was part of a drive toward greater cellular energy flux with as a by-product increased organic carbon exudation, in turn driving co-evolution with co-occurring heterotrophs(55). Added context from our findings here suggests that various adaptations over the course of *Prochlorococcus* evolution collectively mediated an ecological transition from physical-chemical interactions at microscopic scales on particles to primarily chemical interactions at ecosystem scales in the water column.

409 **Materials and Methods**
410
411
412 **Culture conditions for growth curves**
413
414 *Prochlorococcus* or *Synechococcus* cells were grown under constant light flux at 24°C in
415 natural seawater-based Pro99 medium containing 0.2-µm-filtered Sargasso Sea water,
416 amended with Pro99 nutrients (N, P, and trace metals) prepared as previously described
417 (Moore *et al.* 2007). The low light experiment in *Prochlorococcus* MIT9303 and MIT9313
418 was performed at a light level of 1.5 µmol quanta m^{-2} s^{-1}. The other experiments in
419 *Prochlorococcus* or *Synechococcus* were performed at 12 or 15 µmol quanta m^{-2} s^{-1} as
420 specified in each legend. The final concentrations of NH_4^+were 800 µM in Pro99, 250 µM in
421 Pro5, 150 µM in Pro3, and 50 µM in Pro1. In these experiments, half of the samples were
422 amended with high molecular weight chitosan (Millipore Sigma) to a final concentration of
423 56 µg/ml. All the growth curves were performed in triplicates.
424
425 **Identification of genes involved in chitin degradation and peptidoglycan recycling**
426
427 To identify genes potentially involved in chitin-degradation, we searched for homologs to
428 known chitin degradation genes(12) in *Prochlorococcus* strains MIT9313 and MIT1318
429 using blast. Similarly, for peptidoglycan recycling, we searched for homologs to known
430 peptidoglycan recycling genes(17). We found homologues for most genes of the
431 peptidoglycan recycling pathway employed by *E. coli(17)* in *Prochlorococcus*, most of which
432 had previous functional annotations consistent with our findings. We next assigned each of
433 these sequences to NCBI COGs (clusters of orthologous groups)(59) based on reciprocal best
434 hits (Table S1_chitin-cogs)
435 We then expanded these annotations to our entire collection: 623 *Prochlorococcus(60)* and
436 79 *Synechococcus* genomes(61) (Table S1_pro-syn-genomes). Of note, the majority of these
437 genomes were derived from single-cell sequencing projects and often are not complete. The
438 estimated average completeness for genomes in this set is 75%. We first clustered all proteins
439 using mmseqs(62) (--cov-mode 5 -c 0.5), then annotated the cluster representatives with
440 eggNOG-mapper(63) to obtain NCBI COG labels for each cluster, and, finally, crossmatched
441 the clusters with the COG-labels assigned to our seed sequence set. We manually checked
442 and if necessary refined each matched protein cluster for consistency and correct functional
443 assignment. For the final list of annotated genes see (Table S1 pro-chitin-genes).
444
445 **Quantitative PCR analysis**
446
447 *Prochlorococcus* MIT9303 cells grown at 11 µmol photons m^{-2} s^{-1} were collected from the
448 samples by centrifugation in triplicates at each time point and each condition. RNA samples
449 were extracted with a standard acidic Phenol:Chloroform protocol and measured with
450 Nanodrop (Thermo Scientific). RevertAid First Strand cDNA Synthesis Kit (Thermo
451 Scientific) with random primers was used to obtain cDNA. Quantitative PCR reactions were
452 performed in a CFX96 thermocycler (Bio-Rad) using the primers listed in Table S1. The
453 expression of *rnpB* gene was used to normalize the results.
454
455 **Chitinase assay**
456
457 *Prochlorococcus* MIT9303, MIT9313 and *Synechococcus* WH7803 cultures were grown at
458 15 µmol quanta m^{-2} s^{-1} in Pro99 media amended with high molecular weight chitosan

459 (Millipore Sigma) to a final concentration of 56 µg/ml in triplicates. A volume of 50 ml of
460 culture in mid-exponential was then centrifuged to separate the cells fraction and the spent
461 media. The pellet was flash frozen, resuspended in sterile MilliQ water to a volume of 2 ml,
462 sonicated and filtered through a Spin-X centrifuge tube filter (Costar). The supernatant was
463 filtered through a 0.45 µm filter and concentrated using 30kDa Amicon® Ultra-15
464 Centrifugal Filter Units (Millipore) to a volume of 1,5 ml. Half volume of each sample has
465 been boiled at 90°C for 45 minutes to serve as controls. Protease inhibitor (Roche) was added
466 to all samples. Each sample was then divided into 3 aliquots. Each aliquot was tested with
467 one of the 3 substrates contained in the Chitinase kit (Sigma): 4-Methylumbelliferyl N,N′-
468 diacetyl-β-D-chitobioside (substrate suitable for exochitinase activity detection or
469 chitobiosidase activity), 4-Methylumbelliferyl N-acetyl-β-D-glucosaminide (substrate
470 suitable for exochitinase activity detection or β-N-acetylglucosaminidase activity) and 4-
471 Methylumbelliferyl β-D-N,N′,N″-triacetylchitotriose (substrate suitable for endochitinase
472 activity detection).
473 The aliquots were then mixed with each of these substrates, incubated in darkness and the
474 fluorescence of the 4-methyl-umbelliferone released by the chitinase activity in the sample
475 was measured every 24 hours on a plate reader set at excitation 360 nm and emission at 450
476 nm.
477
478 **Beads and microscopy**
479
480 Chitin magnetic beads (NEB Cat#E8036L), or Agarose magnetic beads (Pierce™ Glutathione
481 Magnetic Agarose Beads Thermo Scientific™ Cat#78602) were washed in Pro99 media and
482 size selected using cell strainers. Chitin beads smaller than 40 µm or larger than 100 µm have
483 been discarded during the washes with Pro99. The media enriched with beads has then been
484 inoculated with the *Prochlorococcus* or *Synechococcus* strains of interest, in triplicates in
485 light level of 30 µmol quanta m^{-2} s^{-1} (for MED4 and WH7803) and 11 µmol quanta m^{-2} s^{-1}
486 (for MIT9303 and MIT9313). Growth was monitored using bulk culture fluorescence
487 measured with a 10AU fluorometer (Turner Designs) and samples were collected in late
488 exponential, at a cell density of 10^8. A volume of 1ml of each sample was poured on a
489 35mm Petri dish with 20 mm Glass Bottom Microwell Dish (Mat Tek). To avoid excessive
490 fluorescent signal from floating cyanobacteria, the samples were washed 5 times with fresh
491 media. Floating culture was removed by placing the mini dish on a magnet (to keep the
492 magnetic beads on the bottom) and then substituted with fresh Pro99 media before placing
493 the sample on the scope. Images were taken with a LSM780 Zeiss, capturing the beads on the
494 bright field and the *Prochlorococcus* by its autofluorescence with laser 561.
495
496 **Analysis of the colonized perimeter and cells colonizing pockets**
497
498 To quantify the fraction of cells colonizing the perimeter of chitin or agarose magnetic beads,
499 we wrote a custom analysis script using MATLAB (version R2020a, Mathworks. Code
500 available at https://github.com/jaschwartzman/prochlorococcus). The script segmented the
501 brightfield image of magnetic beads to create a binary mask for the bead perimeter. To
502 account for the fact that chitin magnetic beads are semi-transparent, the mask was created
503 using the gradient of the image, which defines the shadow around the perimeter of the beads.
504 This area was filled and eroded to define the bead center. The center area was subtracted from
505 the total area to define the perimeter zone of the beads. Any cells found in this zone are
506 assumed to be attached to the bead surface. To define cell area, we segmented the
507 accompanying image of cell autofluorescence. Briefly, cells were segmented by defining a
508 linear threshold based on the magnitude of the gradient of the autofluorescence image. This

509 threshold was defined for each day of experimental acquisition, to account for variation in
510 acquisition parameters. For each bead, the perimeter area, and the subset of the perimeter area
511 colonized by cells were quantified. The fraction of the perimeter area colonized was defined
512 by dividing the total perimeter area by the cell area. An assumption of this quantification is
513 that cells from different taxa occupy approximately the same 2-dimensional area.
514
515 The chitin magnetic beads were found to contain pockets, in which we sometimes observed
516 cells. The irregularities and pockets internal to the chitin hydrogel were visible due to the
517 weak autofluorescence of chitin detected in the 561 nm channel and were also identifiable in
518 brightfield images. In the latter scenario, the greater depth of field in the brightfield image
519 creates the possibility that cells are sitting on a surface above a hollow feature. Due to the
520 diverse morphologies of pockets, we were unable to define a consistent set of characteristics
521 to segment these structures using a script. Accordingly, we quantified the number of particles
522 in which we observed cells colonizing internal pockets manually, by counting instances of
523 cells colonizing either a zone with less autofluorescence within a particle and verifying the
524 presence of a pocket in the brightfield image.
525
526 **RNA-Seq and Metabolites analysis**
527
528 *Prochlorococcus* MIT9303 and MIT9313 cells were grown under constant light flux at 11
529 μmol photons m^{-2} s^{-1} at 24°C in artificial AMP1 medium(64). Cultures were transferred to
530 AMP1 from Pro99 and kept in AMP1 for at least 3 transfers before performing the
531 experiment to avoid any potential contributions to observed pathway dynamics by
532 background levels of uncharacterized organic polymers in natural seawater. Half of the
533 samples were supplemented with chitosan (Millipore Sigma) to a final concentration of 56
534 μg/ml. The growth curves were monitored using bulk culture fluorescence measured with a
535 10AU fluorometer (Turner Designs) and the cell count was recorded using Guava®
536 easyCyte™ HT Flow Cytometer. Samples were collected on day 1 and day 3 after inoculation
537 for RNA extraction and day 4 and day 6 for the metabolomics analysis.
538
539 For the RNA-Seq *Prochlorococcus* cells were collected from the samples by centrifugation in
540 triplicates at each time point and each condition. RNA samples were extracted with a
541 standard acidic Phenol:Chloroform protocol, rRNA was depleted with NEBNext® rRNA
542 Depletion Kit (Bacteria); libraries were prepared with KAPA HyperPrep Kit (Roche) and the
543 multiplexed samples were run on an Illumina HiSeq with a 75nt NextSeq sequencing
544 program.
545
546 **RNA-Seq analysis**
547
548 The raw Illumina reads were trimmed of adapters using bbduk v38.16(65) (ktrim=r, k=23,
549 mink=11, hdist=1). Low-quality regions were removed from the adapter-trimmed sequences
550 with bbduk v38.16(65) (qtrim=rl, trimq=6). The trimmed RNA-seq reads from
551 *Prochlorococcus* MIT9303 and MIT9313 cultures were aligned to the MIT9303 and
552 MIT9313 reference genomes, respectively (available from https://github.com/thackl/pro-
553 tycheposons/) with the Burrows-Wheeler Aligner v0.7.16a-r1181(66), using the BWA-
554 backtrack algorithm. The number of reads that aligned to each annotated ORF in the "sense"
555 orientation was determined using the HTSeq package v0.11.2(67) (default parameters,
556 "nonunique all"). Counts of reads that aligned to each ORF (excluding rRNAs and tRNAs)
557 were compiled across replicates. MIT9303 and MIT9313 reads were analyzed separately
558 using the DESeq2 R package v1.24.0(68) to determine differentially expressed genes. The

559 standard DESeq2 functions and workflow were implemented to normalize samples by library
560 sequencing depth and estimate gene dispersion. Differential expression tests were performed
561 on comparisons of cultures with chitosan vs. control cultures one and three days after
562 chitosan addition. Significance was determined with the Wald test, using a negative binomial
563 generalized linear model, and p-values were corrected for multiple testing with the
564 Benjamini–Hochberg procedure. Following the guidance of the DESeq2 authors(68), genes
565 were considered to be significantly differentially expressed between a given pair of
566 treatments if the adjusted p-value was <0.1. Gene expression results were visualized with
567 ggplot2(69).
568
569 **Metabolite extractions**
570
571 For the metabolomics analysis, *Prochlorococcus* cells were filtered under gentle vacuum (to
572 prevent cell lysis) in a glass filtration tower onto 0.1 µM Omnipore filters (Millipore). Filters
573 were then folded and placed into a cryovial, and frozen at -80ºC until processed. We
574 extracted intracellular metabolites using a method described in (70) and modified as
575 described in (71). Briefly, we extracted each filter with ice-cold extraction solvent (40:40:20
576 acetonitrile: methanol: water with 0.1 M formic acid), neutralized the combined extracts with
577 6M ammonium hydroxide, and dried them in a vacufuge until near dryness. Prior to liquid
578 chromatography-mass spectrometry (LC/MS) analysis, we re-constituted all extracts in 245
579 µL of solvent (30 µL MQ pure water, 70 µL methanol, and 145 µL acetonitrile) with
580 isotopically-labeled injection standards (50 pg/µL each; d_2 biotin, d_6 succinic acid, d_4 cholic
581 acid, d_7 indole-3-acetic acid, and $^{13}C_1$-phenylalanine). We generated a pooled sample for
582 quality control (QC) by combining 25 µL aliquots from each sample.
583
584 **LC/MS analysis of metabolites**
585
586 The organic matter extracts were analyzed using targeted LC/MS. A mix of metabolite
587 standards (see Table S4) was made in 80:20 acetonitrile:Milli-Q water at 10 µg/mL. Matrix-
588 matched calibration solutions were prepared by diluting his mix in the pooled sample with
589 methanol and water added to match the composition of the samples. The concentrations
590 prepared included 0.25, 0.5, 2.5, 5, 12.5, 25, 50, 125, 250, and 500 ng/mL. Separate
591 hydrophilic interaction liquid chromatography (HILIC) methods were developed to separate
592 metabolites in negative and positive ionization modes. For negative mode, a 2.1 x 100 mm,
593 2.7 µm Infinity Lab Poroshell HILIC-Z, P column (Agilent Technologies) was used. A
594 mobile phase at pH 9 was prepared for gradient elution with 10 mM ammonium acetate in
595 water (A) and 10 mM ammonium acetate in 90% acetonitrile (B) and pH adjusted with
596 ammonium hydroxide. The additive medronic acid (5 mM methylenediphosphonic acid) was
597 added to A and B at final 5 µM concentration to improve peak shape (72). A sample volume
598 of 5 µL was injected onto the column held at 30 °C, and eluted at a flow rate of 0.3 mL/min
599 with the following gradient: hold at 90% B from 0 to 1.7 min, 90 to 60% from 1.7 to 10 min,
600 hold at 60% B from 10.2 to 12.7 min, return to 90% B at 13.5 min, and equilibrate with 90%
601 B till 20 min. For positive ion mode analysis, a 2.1 x 100 mm, 1.7 um Acquity BEH Amide
602 column (Waters Corporation) was used. A mobile phase at pH 10 was prepared and
603 composed of 0.1% ammonium hydroxide in Milli-Q water (A) and 0.1% ammonium
604 hydroxide in 90% acetonitrile. A 5 µL sample volume was injected onto the column held at
605 40 °C, and eluted at 0.3 mL/min with the same gradient as above. The autosampler was
606 washed between injections to prevent carryover with two successive wash solutions, 50:50
607 acetonitrile/water followed by 95:5 acetonitrile/water.
608

To quantify metabolites, we used liquid chromatography (Accela Open Autosampler and Accela 1250 Pump, Thermo Scientific) coupled to a heated electrospray ionization source (H-ESI) and a triple quadrupole mass spectrometer (TSQ Vantage, Thermo Scientific) operated under selected reaction monitoring (SRM) mode. Optimal SRM parameters (s-lens, collision energy, fragment ions) for each target compound were determined with authentic standards purchased from Sigma. The complete list of metabolites is provided in Table S5. We monitored two SRM transitions per compound for quantification and confirmation and generated external calibration curves based on peak area for each compound. We converted raw data files from proprietary Thermo (.RAW) format to mzML using the msConvert tool(73) prior to processing with El-MAVEN(74). Samples were analyzed in random order within each batch, and the pooled QC sample was analyzed every six injections.

Phylogenetic analysis

Sequences were collected from the Genbank database(75) for the following chitin degradation pathway proteins: The N-terminal region of ChiA/ChiA-like, the C-terminal region of ChiA/ChiA-like, UgpA, UgpE, NagZ, NagK, NagA, and NagB. Orthologs found within *Prochlorococcus* MIT1303 were used as protein search queries using BLASTP(76), with the top 500 or 250 hits recovered in each case. Each set of sequences were then aligned in MAFFT(77) with the automatic algorithm selection option. Aligned sequences were then used for phylogenetic reconstruction using IQTree(78) with automatic best-fitting model selection. All sequence alignment and phylogenetic data files are available in SI data (Data S1, SI Text 1 files), with alignment and tree filenames in each case describing the algorithms and parameters used for these reconstructions. Several BLAST hits for the ChiA and ChiA-like genes in SynPro overlapped, with some protein sequences containing multiple domains homologous to different chitinase orthologs in other bacteria. A phylogenomic analysis of our alignment data showed that the SynPro variant was likely the result of a fusion between genes from Planctomycetes, before or after horizontal gene transfer into SynPro (see SI Text 1 and SI Text 1 files for a detailed analysis of the protein fusion history).

Acknowledgments

We thank members of the Chisholm lab for thoughtful discussions, and Nikolai Radzinski for insightful discussions and useful references regarding microbial aggregation. This reseach was supported by grants from the Simons Foundation (Award ID #509034SCFY20 to R.B. and S.W.C., and SCOPE Award ID 329108 to M.J. Follows; Life Sciences Award IDs 337262, 647135, 736564 to S.W.C.; SCOPE Award ID 329108 and 721246 to S.W.C.). G.C. was also supported by the EMBO Long-Term Fellowship (ALTF 904-2018) and by the Human Frontier Science Program (LT000069/2019-L). This paper is a contribution from the Simons Collaboration on Ocean Processes and Ecology (SCOPE).

Contributions

G.C., R.B., A.Y. and S.W.C. designed experiments.
G.C., J.S., X.L. and A.M. performed experiments.
T.H., E.T. and R.B. performed bioinformatic analyses.
K.L., M.K.S., G.S. and E.B.K. performed metabolite analyses.
G.F. and J.P. performed phylogenetic analyses.
G.C, R.B. and S.W.C. interpreted data.
R.B. developed macroevolutionary model.
R.B., G.C., and S.W.C. wrote the paper with contributions from all authors.

REFERENCES

1. J. B. Waterbury, S. W. Watson, R. R. L. Guillard, L. E. Brand, Widespread occurrence of a unicellular, marine, planktonic, cyanobacterium. *Nature* **277**, 293–294 (1979).

2. S. W. Chisholm, *et al.*, A novel free-living prochlorophyte abundant in the oceanic euphotic zone. *Nature* **334**, 340 (1988).

3. P. Flombaum, *et al.*, Present and future global distributions of the marine Cyanobacteria Prochlorococcus and Synechococcus. *Proc. Natl. Acad. Sci. U. S. A.* **110**, 9824–9829 (2013).

4. G. Gómez-Baena, *et al.*, Glucose uptake and its effect on gene expression in prochlorococcus. *PLoS One* **3**, e3416 (2008).

5. M. C. Muñoz-Marín, *et al.*, Mixotrophy in marine picocyanobacteria: use of organic compounds by Prochlorococcus and Synechococcus. *ISME J.* **14**, 1065–1073 (2020).

6. M. del C. Muñoz-Marín, *et al.*, Prochlorococcus can use the Pro1404 transporter to take up glucose at nanomolar concentrations in the Atlantic Ocean. *Proc. Natl. Acad. Sci. U. S. A.* **110**, 8597–8602 (2013).

7. Z. Wu, *et al.*, Significant organic carbon acquisition by Prochlorococcus in the oceans. *bioRxiv*, 2022.01.14.476346 (2022).

8. J. R. Casey, *et al.*, Basin-scale biogeography of marine phytoplankton reflects cellular-scale optimization of metabolism and physiology. *Science Advances* **8**, eabl4930 (2022).

9. A. P. Yelton, *et al.*, Global genetic capacity for mixotrophy in marine picocyanobacteria. *ISME J.* **10**, 2946–2957 (2016).

10. H.-M. Cauchie, Chitin production by arthropods in the hydrosphere. *Hydrobiologia* **470**, 63–95 (2002).

11. K. W. Tang, V. Turk, H. P. Grossart, Linkage between crustacean zooplankton and aquatic bacteria. *Aquat. Microb. Ecol.* **61**, 261 (2010).

12. S. Beier, S. Bertilsson, Bacterial chitin degradation-mechanisms and ecophysiological strategies. *Front. Microbiol.* **4**, 149 (2013).

13. P. Sánchez-Baracaldo, Origin of marine planktonic cyanobacteria. *Sci. Rep.* **5**, 17418 (2015).

14. M. del M. Aguilo-Ferretjans, *et al.*, Pili allow dominant marine cyanobacteria to avoid sinking and evade predation. *Nat. Commun.* **12**, 1–10 (2021).

15. J. J. Pierella Karlusich, *et al.*, A robust approach to estimate relative phytoplankton cell abundances from metagenomes. *Mol. Ecol. Resour.* (2022) https:/doi.org/10.1111/1755-0998.13592.

16. M. W. Lomas, S. B. Moran, Evidence for aggregation and export of cyanobacteria and nano-eukaryotes

from the Sargasso Sea euphotic zone. *Biogeosciences* **8**, 203–216 (2011).

17. C. Mayer, *et al.*, Bacteria's different ways to recycle their own cell wall. *Int. J. Med. Microbiol.* **309**, 151326 (2019).

18. A. Ebrahimi, J. Schwartzman, O. X. Cordero, Cooperation and spatial self-organization determine rate and efficiency of particulate organic matter degradation in marine bacteria. *Proc. Natl. Acad. Sci. U. S. A.* **116**, 23309–23316 (2019).

19. M. S. Datta, E. Sliwerska, J. Gore, M. F. Polz, O. X. Cordero, Microbial interactions lead to rapid micro-scale successions on model marine particles. *Nat. Commun.* **7**, 11965 (2016).

20. T. N. Enke, *et al.*, Modular Assembly of Polysaccharide-Degrading Marine Microbial Communities. *Curr. Biol.* **29**, 1528–1535.e6 (2019).

21. R. R. Malmstrom, *et al.*, Temporal dynamics of Prochlorococcus ecotypes in the Atlantic and Pacific oceans. *ISME J.* **4**, 1252–1264 (2010).

22. Jiang Haibo, Kong Renqiu, Xu Xudong, The N-Acetylmuramic Acid 6-Phosphate Etherase Gene Promotes Growth and Cell Differentiation of Cyanobacteria under Light-Limiting Conditions. *J. Bacteriol.* **192**, 2239–2245 (2010).

23. Y. Saito, T. Okano, F. Gaill, H. Chanzy, J.-L. Putaux, Structural data on the intra-crystalline swelling of β-chitin. *Int. J. Biol. Macromol.* **28**, 81–88 (2000).

24. L. R. Thompson, *et al.*, Phage auxiliary metabolic genes and the redirection of cyanobacterial host carbon metabolism. *Proc. Natl. Acad. Sci. U. S. A.* **108**, E757–E764 (2011).

25. K. Abe, N. Nomura, S. Suzuki, Biofilms: hot spots of horizontal gene transfer (HGT) in aquatic environments, with a focus on a new HGT mechanism. *FEMS Microbiol. Ecol.* **96** (2020).

26. H.-C. Flemming, S. Wuertz, Bacteria and archaea on Earth and their abundance in biofilms. *Nat. Rev. Microbiol.* **17**, 247–260 (2019).

27. O. Rota-Stabelli, A. C. Daley, D. Pisani, Molecular Timetrees Reveal a Cambrian Colonization of Land and a New Scenario for Ecdysozoan Evolution. *Curr. Biol.* **23**, 392–398 (2013).

28. G. P. Fournier, *et al.*, The Archean origin of oxygenic photosynthesis and extant cyanobacterial lineages. *Proc. Biol. Sci.* **288**, 20210675 (2021).

29. T. H. P. Harvey, M. I. Vélez, N. J. Butterfield, Exceptionally preserved crustaceans from western Canada reveal a cryptic Cambrian radiation. *Proceedings of the National Academy of Sciences* **109**, 1589–1594 (2012).

30. M. Williams, T. R. A. Vandenbroucke, V. Perrier, D. J. Siveter, T. Servais, A link in the chain of the Cambrian zooplankton: bradoriid arthropods invade the water column. *Geol. Mag.* **152**, 923–934 (2015).

31. V. Perrier, M. Williams, D. J. Siveter, The fossil record and palaeoenvironmental significance of marine arthropod zooplankton. *Earth-Sci. Rev.* **146**, 146–162 (2015).

32. T. Servais, *et al.*, The onset of the "Ordovician Plankton Revolution" in the late Cambrian. *Palaeogeogr. Palaeoclimatol. Palaeoecol.* **458**, 12–28 (2016).

33. B. Kröger, T. Servais, Y. Zhang, The origin and initial rise of pelagic cephalopods in the Ordovician. *PLoS One* **4**, e7262 (2009).

34. A. Blieck, The Andre Dumont medallist lecture: from adaptive radiations to biotic crises in palaeozoic vertebrates: a geobiological approach/Des radiations adaptatives aux crises biologiques des vertebres paleozoiques: une approche geobiologique. *Geologica Belgica* **14**, 203+ (2011).

35. K. M. Shoemaker, S. Duhamel, P. H. Moisander, Copepods promote bacterial community changes in surrounding seawater through farming and nutrient enrichment. *Environ. Microbiol.* **21**, 3737–3750 (2019).

36. M. S. Datta, *et al.*, Inter-individual variability in copepod microbiomes reveals bacterial networks linked to host physiology. *ISME J.* **12**, 2103–2113 (2018).

37. R. A. Foster, J. L. Collier, E. J. Carpenter, Reverse transcription pcr amplification of cyanobacterial symbiont 16s rRNA sequences from single non-photosynthetic eukaryotic marine planktonic host cells1. *J. Phycol.* **42**, 243–250 (2006).

38. T. Yuasa, T. Horiguchi, S. Mayama, A. Matsuoka, O. Takahashi, Ultrastructural and molecular characterization of cyanobacterial symbionts in Dictyocoryne profunda (polycystine radiolaria). *Symbiosis* **57**, 51–55 (2012).

39. C. Bird, *et al.*, Cyanobacterial endobionts within a major marine planktonic calcifier (Globigerina bulloides, Foraminifera) revealed by 16S rRNA metabarcoding. *Biogeosciences* **14**, 901–920 (2017).

40. T. Nakayama, *et al.*, Single-cell genomics unveiled a cryptic cyanobacterial lineage with a worldwide distribution hidden by a dinoflagellate host. *Proc. Natl. Acad. Sci. U. S. A.* **116**, 15973–15978 (2019).

41. M. Kim, D. H. Choi, M. G. Park, Cyanobiont genetic diversity and host specificity of cyanobiont-bearing dinoflagellate Ornithocercus in temperate coastal waters. *Sci. Rep.* **11**, 1–13 (2021).

42. T. Bosak, B. Liang, M. S. Sim, A. P. Petroff, Morphological record of oxygenic photosynthesis in conical stromatolites. *Proc. Natl. Acad. Sci. U. S. A.* **106**, 10939–10943 (2009).

43. C. E. Blank, P. Sánchez-Baracaldo, Timing of morphological and ecological innovations in the cyanobacteria--a key to understanding the rise in atmospheric oxygen. *Geobiology* **8**, 1–23 (2010).

44. S. V. Lalonde, K. O. Konhauser, Benthic perspective on Earth's oldest evidence for oxygenic photosynthesis. *Proc. Natl. Acad. Sci. U. S. A.* **112**, 995–1000 (2015).

45. H.-C. Flemming, *et al.*, Biofilms: an emergent form of bacterial life. *Nat. Rev. Microbiol.* **14**, 563–575 (2016).

46. R. Allen, B. E. Rittmann, R. Curtiss 3rd, Axenic biofilm formation and aggregation by Synechocystis sp. Strain PCC 6803 are induced by changes in nutrient concentration and require cell surface structures. *Appl. Environ. Microbiol.* **85** (2019).

47. C. Callieri, A. Lami, R. Bertoni, Microcolony formation by single-cell Synechococcus strains as a fast response to UV radiation. *Appl. Environ. Microbiol.* **77**, 7533–7540 (2011).

48. S. Klähn, C. Steglich, W. R. Hess, M. Hagemann, Glucosylglycerate: a secondary compatible solute common to marine cyanobacteria from nitrogen-poor environments. *Environ. Microbiol.* **12**, 83–94 (2010).

49. C. E. Blank, Phylogenetic distribution of compatible solute synthesis genes support a freshwater origin for cyanobacteria. *J. Phycol.* **49**, 880–895 (2013).

50. G. C. Kettler, *et al.*, Patterns and implications of gene gain and loss in the evolution of Prochlorococcus. *PLoS Genet.* **3**, e231 (2007).

51. F. Partensky, L. Garczarek, Prochlorococcus: advantages and limits of minimalism. *Ann. Rev. Mar. Sci.* **2**, 305–331 (2010).

52. A. Dufresne, L. Garczarek, F. Partensky, Accelerated evolution associated with genome reduction in a free-living prokaryote. *Genome Biol.* **6**, R14 (2005).

53. B. A. S. Van Mooy, G. Rocap, H. F. Fredricks, C. T. Evans, A. H. Devol, Sulfolipids dramatically decrease phosphorus demand by picocyanobacteria in oligotrophic marine environments. *Proc. Natl. Acad. Sci. U. S. A.* **103**, 8607–8612 (2006).

54. J. J. Grzymski, A. M. Dussaq, The significance of nitrogen cost minimization in proteomes of marine microorganisms. *ISME J.* **6**, 71–80 (2012).

55. R. Braakman, M. J. Follows, S. W. Chisholm, Metabolic evolution and the self-organization of ecosystems. *Proc. Natl. Acad. Sci. U. S. A.* **114**, E3091–E3100 (2017).

56. H. Luo, Y. Huang, R. Stepanauskas, J. Tang, Excess of non-conservative amino acid changes in marine bacterioplankton lineages with reduced genomes. *Nature Microbiology* **2**, 1–9 (2017).

57. C. S. Ting, C. Hsieh, S. Sundararaman, C. Mannella, M. Marko, Cryo-electron tomography reveals the comparative three-dimensional architecture of Prochlorococcus, a globally important marine cyanobacterium. *J. Bacteriol.* **189**, 4485–4493 (2007).

58. N. Cermak, *et al.*, High-throughput measurement of single-cell growth rates using serial microfluidic mass sensor arrays. *Nat. Biotechnol.* **34**, 1052–1059 (2016).

59. M. Y. Galperin, K. S. Makarova, Y. I. Wolf, E. V. Koonin, Expanded microbial genome coverage and improved protein family annotation in the COG database. *Nucleic Acids Res.* **43**, D261–9 (2015).

60. T. Hackl, *et al.*, Novel integrative elements and genomic plasticity in ocean ecosystems. *bioRxiv*, 2020.12.28.424599 (2020).

61. S. L. Hogle, *et al.*, Siderophores as an iron source for picocyanobacteria in deep chlorophyll maximum layers of the oligotrophic ocean. *ISME J.*, 1–11 (2022).

62. M. Steinegger, J. Söding, Clustering huge protein sequence sets in linear time. *Nat. Commun.* **9**, 2542 (2018).

63. J. Huerta-Cepas, *et al.*, eggNOG 5.0: a hierarchical, functionally and phylogenetically annotated orthology resource based on 5090 organisms and 2502 viruses. *Nucleic Acids Res.* **47**, D309–D314 (2019).

64. L. R. Moore, *et al.*, Culturing the marine cyanobacterium Prochlorococcus. *Limnol. Oceanogr. Methods* **5**, 353–362 (2007).

65. B. Bushnell, BBTools software package. *URL http://sourceforge. net/projects/bbmap* (2014).

66. H. Li, R. Durbin, Fast and accurate short read alignment with Burrows-Wheeler transform. *Bioinformatics* **25**, 1754–1760 (2009).

67. S. Anders, P. T. Pyl, W. Huber, HTSeq—a Python framework to work with high-throughput sequencing data. *Bioinformatics* **31**, 166–169 (2015).

68. M. I. Love, W. Huber, S. Anders, Moderated estimation of fold change and dispersion for RNA-seq data with DESeq2. *Genome Biol.* **15**, 550 (2014).

69. H. Wickham, ggplot2. *WIREs Comp Stat* **3**, 180–185 (2011).

70. J. D. Rabinowitz, E. Kimball, Acidic Acetonitrile for Cellular Metabolome Extraction from Escherichia coli. *Anal. Chem.* **79**, 6167–6173 (2007).

71. M. C. Kido Soule, K. Longnecker, W. M. Johnson, E. B. Kujawinski, Environmental metabolomics: Analytical strategies. *Mar. Chem.* **177**, 374–387 (2015).

72. J. J. Hsiao, O. G. Potter, T.-W. Chu, H. Yin, Improved LC/MS Methods for the Analysis of Metal-Sensitive Analytes Using Medronic Acid as a Mobile Phase Additive. *Anal. Chem.* **90**, 9457–9464 (2018).

73. M. C. Chambers, *et al.*, A cross-platform toolkit for mass spectrometry and proteomics. *Nat. Biotechnol.* **30**, 918–920 (2012).

74. S. Agrawal, *et al.*, El-MAVEN: A Fast, Robust, and User-Friendly Mass Spectrometry Data Processing Engine for Metabolomics. *Methods Mol. Biol.* **1978**, 301–321 (2019).

75. D. A. Benson, *et al.*, GenBank. *Nucleic Acids Res.* **46**, D41–D47 (2018).

76. S. F. Altschul, W. Gish, W. Miller, E. W. Myers, D. J. Lipman, Basic local alignment search tool. *J. Mol. Biol.* **215**, 403–410 (1990).

77. K. Katoh, K.-I. Kuma, H. Toh, T. Miyata, MAFFT version 5: improvement in accuracy of multiple sequence alignment. *Nucleic Acids Res.* **33**, 511–518 (2005).

78. L.-T. Nguyen, H. A. Schmidt, A. von Haeseler, B. Q. Minh, IQ-TREE: A Fast and Effective Stochastic Algorithm for Estimating Maximum-Likelihood Phylogenies. *Mol. Biol. Evol.* **32**, 268–274 (2014).